TITLE:

Schematic model for induced fission in a configuration-interaction approach

AUTHOR(S):

Uzawa, K.; Hagino, K.

Schematic model for induced fission in a configuration-interaction approach

K. Uzawa and K. Hagino

Department of Physics, Kyoto University, Kyoto 606-8502, Japan

We model fission at barrier-top energies in a simplified model space that permits comparison of different components of the residual nucleon-nucleon interaction. The model space is built on particle-hole excitations of reference configurations. These are Slater determinants of uniformly spaced orbitals characterized only by their quantum numbers and orbital energies. The residual interaction in the Hamiltonian includes the diabatic interaction connecting similar orbitals at different deformations, the pairing interaction between like nucleons, and a schematic off-diagonal neutron-proton interaction. We find that the fission reaction probability is sensitive to the off-diagonal neutron-proton interaction much more than to the pairing and the diabatic interactions. In particular, the transmission coefficients become insensitive to the strength of the pairing interaction when the neutron-proton interaction is large. We also find that the branching ratio is insensitive to the final-state scission dynamics, as is assumed in the well-known Bohr-Wheeler theory.

I. INTRODUCTION

Nuclear fission was discovered about 80 years ago [1,2]. Many phenomenological models have been proposed since then and have successfully explained the observed behavior. A well-known model is of Bohr and Wheeler [3], in which a statistical treatment is implemented under the transition-state hypothesis. In addition to this model, the statistical models based on the Hauser-Feshbach theory [4] as well as dynamical models based on a transport theory [5–7] have also played an important role [8]. In contrast, a microscopic understanding of induced fission has still been far from complete. This has been regarded as one of the most challenging subjects in many-fermion quantum dynamics, and in fact in a recent review for future directions of fission theory [9], the authors omitted this topic because there has been virtually no coherent microscopic theory addressing this question up to now.

In this paper, we apply the configuration-interaction (CI) approach [10,11] to a schematic model in order to discuss the role of various types of nucleon-nucleon interaction. In this approach, many-particle-many-hole configurations at different nuclear deformations are coupled by residual interactions. Those many-body configurations are constructed in a constrained mean-field potential at each deformation. The configuration space includes particle-hole excitations of the reference configurations and thus greatly extends the space accessed by the collective coordinates defined in the usual generator coordinate method (GCM) [12]. See Ref. [13] for a similar approach.

In a recent publication [11], the CI approach was applied to semirealistic calculations based on the Skyrme energy functional. However, for simplicity, several simplifications were introduced. In particular, the model space was restricted to neutron excitations only with seniority zero. As a consequence, only two types of interaction were needed, namely, the pairing and the diabatic interactions. In nuclear

structure the off-diagonal neutron-proton interaction is important as well, but its role in low-energy nuclear fission has not yet been clarified.

In this paper, we apply the CI approach to a schematic model with uniformly spaced single-particle orbitals. A preliminary version of the work can be found in Ref. [14]; some of the Supplemental Material of that work is included in Appendix A of this paper. While the model presented here is still far from realistic, our schematic treatment of the configuration space and the details of the Hamiltonian may be useful for focusing attention on aspects of those ingredients in a more quantitative theory. This is especially needed in light of the huge CI spaces required to describe the large changes of deformation that occur in fission.

The paper is organized as follows: Section II presents the theoretical framework and the model Hamiltonian based on uniformly spaced orbital energies. In Sec. III we apply the model to transmission across a barrier. There are three kinds of residual interaction that can mediate the transmission dynamics, and we examine their relative importance. The interaction types are diabatic, pairing, and the fully off-diagonal nucleon-nucleon interaction. Taking the model as a schematic treatment of fission, we examine in Sec. IV the branching ratio between fission and the capture. It is shown that one of the tenets of the Bohr-Wheeler theory (insensitivity to fission partial widths) can be achieved with the model Hamiltonian. We then summarize the paper in Sec. V.

II. CONFIGURATION-INTERACTION APPROACH TO INDUCED FISSION

A. Transmission coefficient

In the present approach, the reference configurations are defined at discrete points along the fission path. Many-particle-many-hole excited states are then generated from those reference configurations to form subspaces in the

configuration space which we call Q blocks. In general, the states in different Q blocks are not orthogonal to each other, and one needs to consider the norm matrix N with matrix elements $\langle qj|q'j'\rangle$ where q and q' label the Q blocks and j, j' are labels for the configurations within a Q block. Similarly, the elements of Hamiltonian matrix H are $\langle qj|H|q'j'\rangle$. Note that, in the usual GCM one takes only the local ground state at each q. In contrast, induced fission is a decay process of an excited nucleus, and it is essential to include excited configurations.

The S-matrix reaction theory also requires matrices Γ_c for decay widths to each channel c. Note that these matrices have the same dimension as the configuration space and may have off-diagonal matrix elements. The present model includes neutron entrance channels, multiple γ-ray capture channels, and multiple fission channels; the corresponding matrices are Γ_n, Γ_{cap}, and Γ_{fis}, respectively. Specific forms of those matrices are given in Sec. II D below.

Based on the Datta formula from S-matrix reaction theory [15–17], we evaluate the transmission coefficient from the incoming channel a to a decay channel b at energy E as

$$T_{a,b}(E) = \sum_{i\in a, j\in b} |S_{i,j}(E)|^2 = \mathrm{Tr}[\Gamma_a G(E) \Gamma_b G(E)^\dagger], \quad (1)$$

where

$$G(E) = [H - i(\Gamma_n + \Gamma_{\mathrm{cap}} + \Gamma_{\mathrm{fis}})/2 - NE]^{-1} \quad (2)$$

is the Green's function with the total width $\Gamma = \Gamma_n + \Gamma_{\mathrm{cap}} + \Gamma_{\mathrm{fis}}$.

In a low-energy induced fission, the channel a corresponds to the incident channel and thus $\Gamma_a = \Gamma_n$, while the exit channel b is either the capture channel or the fission channel.

In GCM calculations for nuclear spectroscopy, it is well known that the non-orthogonality of a basis set often leads to a numerical instability [12,18]. One can largely avoid this problem in reaction calculations because a rather coarse mesh along the fission path provides an acceptable accuracy for estimating the transmission coefficients [10].

B. Model Hamiltonian

The Hamiltonian for each Q block is constructed as

$$H_q = V(q) + H_{\mathrm{sp}} + H_{\mathrm{pair}} + H_{\mathrm{ran}}, \quad (3)$$

where $V(q)$ is the energy of the local ground state at q. Ideally, it is calculated by constrained Hartree-Fock or density-functional theory (DFT). H_{sp}, H_{pair}, and H_{ran} are the single-particle Hamiltonian, the pairing interaction, and the random neutron-proton interaction, respectively.

The configuration space is built in the usual way, defining configurations as Slater determinants of nucleon orbitals. In this paper, we employ a model having a uniform spectrum of orbital energies with a spacing d for both protons and neutrons. The ladder of orbital states extends infinitely in both directions above and below the Fermi surface but is restricted by later truncation of the CI space. The operator for the particle-hole excitation energy E_{ph} is given by

$$H_{sp} = d \sum_{\alpha:n_a>0} n_\alpha a_\alpha^\dagger a_\alpha + d \sum_{\alpha:n_a<0} n_\alpha a_\alpha a_\alpha^\dagger. \quad (4)$$
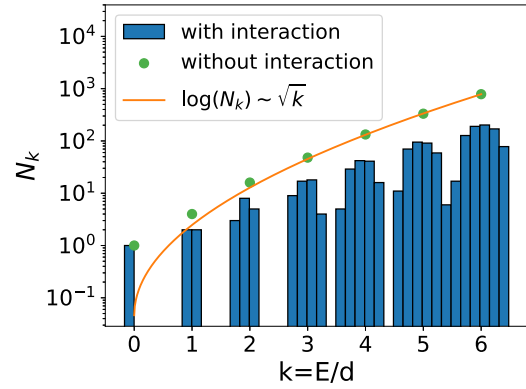

FIG. 1. Spectrum of many-body configurations in the uniform spacing model. N_k denotes the number of $K_{\mathrm{tot}} \equiv \sum K = 0$ configurations at the excitation energy $E = kd$. The green circles show the noninteracting spectrum, while the orange curve shows its fit to the functional form of $N_k = \exp(a\sqrt{k} + b)$ with $a = 3.97$ and $b = -3.06$. The blue filled histograms show the interacting spectrum, obtained by diagonalizing the Hamiltonian H_q with $G_{\mathrm{pair}} = 0$ and $v_{np} = 0.03d$.

The label α includes q and an index ν of orbitals associated with the reference configuration. The interaction matrix elements also require access to the conserved quantum numbers of orbitals. In general, these include parity π, isospin t_z, and angular momentum K about the symmetry axis if there is one. To keep the model as transparent as possible, we ignore parity and assign K to the restricted range $\pm 1/2$.

The orbital excitation energies of many-particle configurations are integral multiples of d given by $E_{\mathrm{ex}} = kd$. As a function of k, the multiplicity of configurations having $K_{\mathrm{tot}} \equiv \sum K = 0$ and $\sum t_z = 0$ is $N_k = (1, 4, 16, 48, 133, 332, 784, \dots)$ for $k = (0, 1, 2, 3, 4, 5, 6, \dots)$. The spectrum up to $k = 6$ is shown in Fig. 1. The orange curve shows a smoothed level density fit to the leading-order dependence on energy as derived from statistical theory. This will provide a way to fit the parameter d to experimental level densities: the single-particle level spacing d sets the energy scale in the model, and other energy parameters will be expressed in units of d. Even though we will not specify the value of d in this paper, d is estimated to be around 0.5 MeV for nuclei in the actinide region [14] (see Appendix A-1).

For residual interactions, both particle-particle (pp) and particle-hole (ph) interactions appear. For the pp residual interaction, we employ a monopole pairing interaction between identical nucleons,

$$H_{\mathrm{pair}} = -G_{\mathrm{pair}} \sum_{\nu\neq\nu'} a_{\nu'}^\dagger a_{\bar{\nu}'}^\dagger a_{\bar{\nu}} a_\nu. \quad (5)$$

Here $a_\nu^\dagger$ is the creation operator of the orbital ν, and $\bar{\nu}$ denotes the time-reversal orbital of ν. The strength of the pairing interaction G_{pair} is around 0.1 MeV in the actinide region [19], corresponding to $G_{\mathrm{pair}} \approx 0.2d$ in the energy units in the present model. In this paper we take $G_{\mathrm{pair}} = 0.3d$ as the baseline value, to be varied to study how the observables depend on the interaction types.

When the monopole pairing interaction is used in the uniform spacing model, the Hamiltonian matrix tends to be singular due to the high degeneracy of the spectrum. In actual numerical calculations, an unphysical divergent behavior may easily appear in the transmission coefficients even if the matrix itself is invertible. To avoid this problem, we add a small random number to the diagonal part of the Hamiltonian kernel as [20]

$$kd \rightarrow kd + 0.1rd,$$

where r is a random number of unit variance taken from a Gaussian ensemble.

For the ph-type residual interaction, we employ a random interaction in the form of

$$H_{\mathrm{ran}} = -v_{np} \sum r a_{\alpha 1}^{\dagger} a_{\alpha 2}^{\dagger} a_{\alpha 4} a_{\alpha 3}, \qquad (6)$$

where the parameter v_{np} is the strength of the interaction and r is a random number, as before. The sum α is restricted to the combinations satisfying $K_1 + K_2 = K_3 + K_4$. An early study has suggested that a neutron-proton interaction is dominant in a diffusion process compared with the one between identical particles [21]. We therefore assume that the interaction H_{ran} acts only on neutron-proton pairs.

Following Appendix A 3, we take $v_{np} = 0.03d$ as a base value in the following calculations. The assumption that the neutron-proton interaction is Gaussian distributed is certainly not justified for the low-energy states in a Q block where collective excitations can be built up. However, high in the spectrum the mixing approaches the random matrix limit. Note that the pairing interaction acts coherently while the random interaction acts incoherently. Our interest is to clarify the role of these two different types of interaction in the transmission process.

Because of the random component in the Hamiltonian, one needs to take an ensemble average to obtain physical quantities. In the following calculations, we take many samples so that the standard deviation becomes smaller than 1%.

C. Off-diagonal couplings

The interaction between different Q blocks is responsible for a shape change and is thus crucial to the modeling. It is clear that the interaction is somewhat suppressed due to the imperfect overlap of orbitals built on different mean-field reference states. The size of the suppression is determined by the overlap kernel, $N(qj, q'j')$, which is given by a determinant of orbital overlaps. For simplicity, we assume that the change of the single-particle orbitals between nearby reference configurations is small. With this assumption, the configurations with the same index j in neighboring Q blocks are diabatically connected with the overlap matrix elements approximated by

$$\langle q\, j | N | q'\, j' \rangle = N(q, q') \delta_{j, j'}, \qquad (7)$$

where $N(q, q')$ is the overlap between the reference configurations.

Based on the idea of the Gaussian overlap approximation (GOA) [12], we parametrize it as

$$N(q, q') = \exp(-\lambda (q - q')^2). \qquad (8)$$

In the main calculations below, we take the value $\lambda = 1.0$ for the overlap between neighboring Q blocks. This sets the numerical scale for q as a distance measure along the fission path. We also consider the model in which the configurations are all orthogonal.

The Hamiltonian kernel $H(qj, q'j')$ can be calculated in a similar manner by assuming that the orbital wave functions are nearly the same in the two reference configurations. To take into account the imperfect overlap of the references states, we multiply the bare matrix elements by the suppression factor $N(q, q')$ to the matrix elements. In addition, one has to take into account the diabatic interaction between those configurations which are connected diabatically. A simple formula for the diabatic interaction has been derived in Ref. [22] based on a self-consistent separable interaction. Based on the GOA, the formula reads

$$\frac{\langle qj | v_{db} | q'j \rangle}{\langle q | q' \rangle} = \frac{E(qj) + E(q'j)}{2} - h_2 (q - q')^2, \qquad (9)$$

where $E(qj) = k_j d + V(q)$ is the energy of the configuration (qj). In the previous work [11], the value of h_2 was estimated to be about 1.5 MeV with the Gogny HFB calculations for ^{236}U. A typical value of single-particle spacing d is around 0.5 MeV when it is corrected for the effective mass (see Table III in Appendix A). Combining these together, we estimate $h_2 = 3d$ in this model.

The first term on the right hand side of this equation ensures that the Green's function (2) transforms properly under a shift in energy scale $E' = E - \epsilon$, that is $G'(E') = G(E)$.

D. Width matrices

The matrices Γ_a ($a = n$, cap, and fis) in Eq. (2) can be in principle derived with the generalized Fermi golden rule [23]

$$(\Gamma_a)_{kk'} = 2\pi \sum_{l \in a} \langle k | v | l \rangle \langle k' | v | l \rangle \delta(E_l - E), \qquad (10)$$

where l labels states in the decay channel a. Due to the nonorthogonality of the configurations, the matrix Γ_a is in general nondiagonal. In this work, we take a separable approximation and parametrize it as[1]

$$(\Gamma_a)_{kk'} = \gamma_a \sum_{l \in a} (N^{1/2})_{k,l} (N^{1/2})_{k',l}, \qquad (11)$$

where $(N^{1/2})_{k,l}$ is the square root of the norm kernel and γ_a is the mean decay width. Here, the indices k and l label both the deformation q and the excitation j. See Appendix B for a derivation of Eq. (11).

---

[1]In Ref. [10], we used N instead of $N^{1/2}$ in the decay matrices. We consider that $N^{1/2}$ is a more physical choice because of the connection to orthogonal bases as we discuss in Appendix B.

III. RESULTS

Let us now numerically evaluate the transmission coefficients and discuss the dynamics of induced fission. To this end, we consider a chain of three Q blocks, $q = q_{-1}, q_0$, and q_1, with the same spacing Δq, that is, $q_{\pm 1} = q_0 \pm \Delta q$. We set them to $q = -1, 0$, and 1 for convenience. Thus the overlaps between adjacent Q blocks is $N(q, q \pm 1) = e^{-1}$ by Eq. (8) with the chosen value of λ. For the barrier, we set $V(q = \pm 1) = 0$ and $V(q = 0) = 4d$, giving a barrier height $B_h = 4d$. In each Q block, the energy cutoff for the many-body configurations is set to be $E_{\text{cut}} = V(q) + 5.5d$. The neutron absorption and the gamma decay occur prior to the fission barrier, so the incident and the capture channels couple to the internal states by Eq. (11) at $q = -1$. Likewise, the fission channel is coupled at $q = 1$. All the states at these endpoints are coupled to individual decay channels. Since the relation $\Gamma_n < \Gamma_{\text{cap}} < \Gamma_{\text{fis}}$ is known empirically in the actinide region [24], we set $\gamma_n = 0.001d$, $\gamma_{\text{cap}} = 0.01d$, and $\gamma_{\text{fis}} = 0.1d$ in the following calculations. As we show in Sec. IIIC below, the transmission dynamics is not sensitive to the value of γ_{fis}.

A. Orthogonal basis

We first consider the case where all configurations are orthogonal so that the norm kernel reads

$$\langle q \, j | N | q' \, j' \rangle = \delta_{q,q'} \delta_{j,j'}. \tag{12}$$

In this case, the suppression factor in the off-diagonal couplings are disregarded; that is, the off-diagonal couplings are fully taken into account without the suppression factor. This is a useful limit to study the role of the pairing interaction, since the diabatic interaction does not contribute.

It is a well-known fact that the pairing correlation modifies drastically the dynamics of spontaneous fission, particularly through a reduction of the collective mass [25–27]. Another important aspect of the pairing correlation is that it is responsible for a hopping of Cooper pairs from one configuration to the neighboring one [28]. On the other hand, the role of pairing correlation in induced fission has not yet been understood well, partly because the pairing correlation is considered to be effective only in the vicinity of the ground state. However, odd-even staggerings have been observed in fission fragments in low-energy induced fission, which suggests that the pairing correlation cannot be completely ignored.

Figure 2 shows the transmission coefficients for the fission channel, calculated with two different values of G_{pair}. The strength of the neutron-proton random interaction is set to be $v_{np} = 0.03d$. One can see that the pairing correlation enhances the transmission probabilities far below the barrier, while its effect is not important at the barrier top and above. This is to be expected, since the number of configurations with high seniority numbers increases as the excitation energy increases and the pairing correlation becomes weaker.

To study systematically the role of pairing in induced fission, we introduce an energy-averaged transmission coefficient. It is defined as

$$\langle T_{n,\text{fis}}(E) \rangle = \frac{1}{\Delta E} \int_{E - \Delta E/2}^{E + \Delta E/2} dE' \, T_{n,\text{fis}}(E'). \tag{13}$$
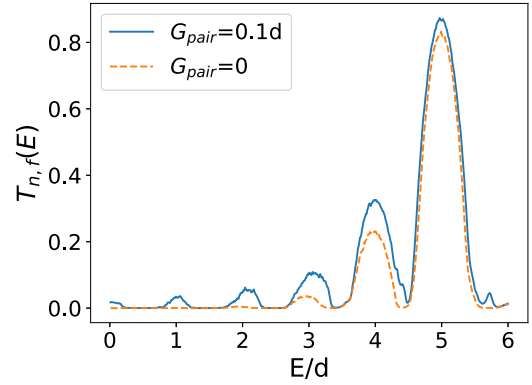

FIG. 2. The transmission coefficients from the incident channel to the fission channel as a function of the excitation energy, E, in the model with an orthogonal configuration space. The solid and the dashed lines are obtained with $G_{\text{pair}} = 0$ and $0.1d$, respectively, for the strength of the pairing interaction. The strength of the neutron-proton interaction and the barrier height are set to be $v_{np} = 0.03d$ and $B_h = 4d$, respectively.

Table I summarizes the energy averaged transmission coefficient at $E = B_h = 4d$ for several sets of $(v_{np}, G_{\text{pair}})$. The energy window for the energy average is set to be $\Delta E = d$. Without the neutron-proton interaction; that is, $v_{np} = 0$, the fission probability increases as the pairing strength increases. Note especially that the transmission coefficient $\langle T_{n,\text{fis}}(E) \rangle$ is zero when there is no interaction at all. As the value of v_{np} increases, the dependence of $\langle T_{n,\text{fis}}(E) \rangle$ on G_{pair} becomes milder. For $v_{np} = 0.06d$, the transmission coefficient is almost insensitive to the value of G_{pair}. This suggests that induced fission is more sensitive to the neutron-proton random interaction as compared with the coherent pairing interaction.

B. Nonorthogonal basis

Let us now examine the dependence on the interactions for a model having a nonorthogonal basis. In this case, diabatically connected configurations have a off-diagonal coupling due to the one-body terms in the Hamiltonian, in addition to the couplings due to the two-body residual interactions. This corresponds to the diabatic interaction (9) parametrized with a quantity h_2. To avoid an artifact due to the degeneracy of the single-particle energies, we introduce an offset energy to the $q = 1$ block, taking $V(q)/d = (0, 4, 0.5)$ in Eq. (3). We mention that this problem appears much more prominently

TABLE I. The averaged transmission coefficient for a fission process, $\langle T_{n,\text{fis}} \rangle$, for several sets of the interaction parameters and assuming that the configurations are orthogonal. The barrier height and the incident energy are both set to be $4d$.

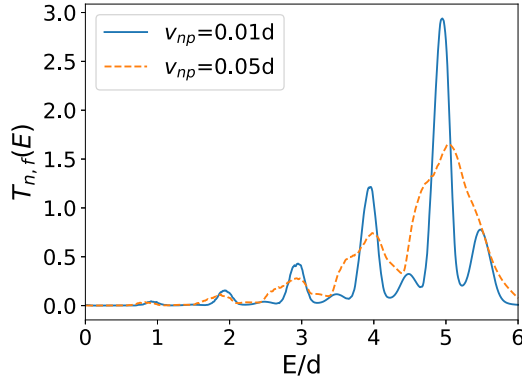| Model	v_{np}	G_{pair}		
		0	0.1d	0.2d
I	0	0	0.0441	0.0589
II	0.03d	0.107	0.161	0.173
III	0.06d	0.318	0.331	0.331

FIG. 3. The transmission coefficient $T_{n,\text{fis}}(E)$ with two different values of v_{np}. The pairing interaction is set to zero, i.e., $G_{\text{pair}} = 0$. The other parameters are $\lambda = 1.0$, $h_2 = 3d$, and $B_h = 4d$.

with the nonorthogonal basis as compared with calculations with the orthogonal basis, which could not be cured merely by introducing random numbers to the Hamiltonian kernel.

Figure 3 shows the transmission probability for fission with two different values of v_{np}. In these calculations, the pairing interaction is switched off by setting $G_{\text{pair}} = 0$, while the parameter h_2 for the diabatic transitions is set to be $3d$. From the figure, one notices that the peaks are lowered and broadened as the value of v_{np} increases. This can be understood easily since the random interaction spreads the spectrum in each Q block as is indicated in Fig. 1. The effect of v_{np} is not only to broaden the peaks in the transmission coefficients but also to increase the energy averaged transmission coefficients, as will be discussed in Table II below.

Figure 4 shows an average fission-to-capture branching ratio α^{-1} as a function of the energy E. We define the average as

$$\alpha^{-1} = \frac{\int dE'\, T_{n,\text{fis}}(E')}{\int dE'\, T_{n,\text{cap}}(E')}, \tag{14}$$

where the range of the integration is the same as that in Eq. (13). To simplify the discussion, we once again set the pairing interaction to be zero. The solid and the dashed lines

TABLE II. The transmission coefficient for fission $\langle T_{n,\text{fis}}\rangle$ and the branching ratio α^{-1} for several sets of interactions. The parameters shown for models I–V1 are the only ones that differ from the base model. The overlap parameter is $\lambda = 1.0$ and the averaged observables are calculated at a central energy $E = 4d$. Interaction strength parameters are in units of d. For model VI, the GCM Hamiltonian is constructed such that the orthogonal physical Hamiltonian Eq. (B15) is diagonal.

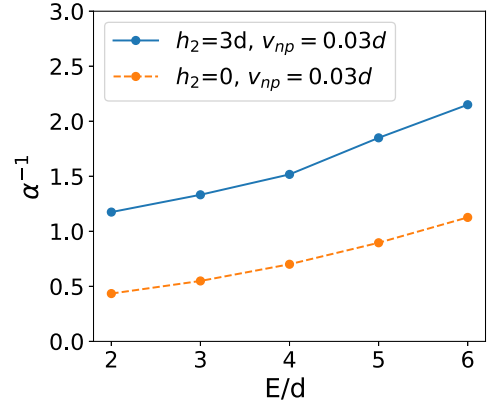| Model	v_{np}	G_{pair}	h_2	$\langle T_{n,\text{fis}}\rangle$	α^{-1}
Base	0.03	0.3	3	0.417	1.62
I		0.0		0.413	1.49
II	0.0			0.372	1.14
III	0.05			0.429	2.27
IV			0.0	0.294	0.739
V	0.0	0.0	0.0	0.172	0.291
VI	0.0	0.0	0.0	0.000	0.000

FIG. 4. The average fission-to-capture branching ratios as a function of the energy with two different values of h_2. The random neutron-proton interaction is taken into account with the strength of $v_{np} = 0.03d$, while the pairing interaction is set to be zero.

are obtained with $h_2 = 3d$ and $h_2 = 0$, respectively. The branching ratios increase with the excitation energy, and we confirmed that the energy dependence becomes stronger as the number of Q blocks increases. This would be an expected behavior from a quantum barrier transmission. Furthermore, one sees that the diabatic interaction increases the branching ratios, that is consistent with the result in Ref. [11].

Table II summarizes the transmission coefficients and the branching ratios for several parameter sets. The results of models I, II, and III indicate that both the neutron-proton interaction and the pairing interaction enhance the transmission coefficients as well as the branching ratios. They also indicate that the transmission coefficients are more sensitive to the neutron-proton interaction than to the pairing interaction. This is consistent with the results of the orthogonal basis shown in Table I, even though the degree of enhancement is smaller than in Table I due to the overlap factor $N(qj, q'j')$ in the off-diagonal matrix elements. In model IV, h_2 is set to be zero. The result indicates that the transmission coefficient and the branching ratio significantly decreases without the diabatic transitions, as has been already observed in Ref. [11]. See also Fig. 4 for the sensitivity of the branching ratios to the value of h_2. Finally, in model V, all the interaction strengths v_{np}, G_{pair}, and h_2 are set to zero. Even in this case, the transmission coefficient is not zero because the corresponding Hamiltonian in the orthogonal physical basis is not diagonal in this case. As we show in Appendix B, one can actually construct the GCM Hamiltonian which is diagonal with the orthogonal basis. With such a GCM Hamiltonian, we have confirmed that the transmission coefficient becomes zero within the numerical error (see model VI in the table).

C. Validity of the transition-state hypothesis

In the Bohr-Wheeler theory for induced fission [3], the decay width is calculated as a sum of transmission coefficients T_i across the barrier via transition states i,

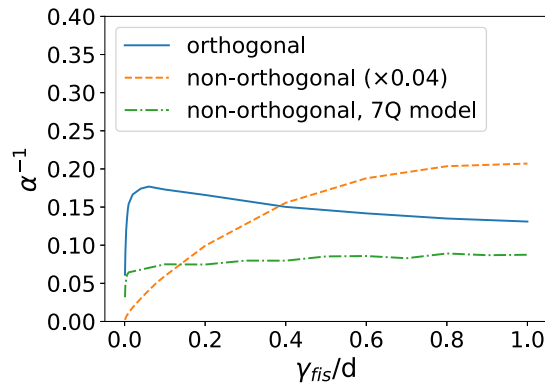$$\Gamma_{\text{BW}} = \frac{1}{2\pi\rho}\sum_i T_i, \tag{15}$$

FIG. 5. The branching ratios at $E = 4d$ as a function of γ_{fis}. The interaction strengths are $(v_{pn}, G_{\text{pair}}, h_2) = (0.03, 0.3, 3)d$. A parabolic fission barrier is employed with the barrier height of $4d$. The solid and the dashed lines show the results of the $3Q$ model, while the dot-dashed line shows the results of the $7Q$ model. While the nonorthogonality of the configurations is neglected in the solid line, it is taken into account in the other lines with $\lambda = 1.0$. For the sake of presentation, the branching ratios are multiplied by factors of 0.2 and 0.04 for the solid and the dashed lines, respectively.

where ρ is the level density of a compound nucleus. The formula indicates that the transition states entirely determine the decay rate, and that the details of the dynamics after crossing the barrier are unimportant. The branching ratio in the Bohr-Wheeler theory would be expressed as

$$\alpha^{-1}(E) = \frac{1}{2\pi \rho(E)\Gamma_{\text{cap}}} \sum_i T_i. \tag{16}$$

The solid and the dashed lines in Fig. 5 show the branching ratios at $E = 4d$ as a function of γ_{fis} for a model with the pairing interaction switched off. For the calculations with the orthogonal basis shown by the solid line, the branching ratio is almost independent of the fission decay width γ_{fis}, in agreement with the insensitivity property of the Bohr-Wheeler theory. On the other hand, with the nonorthogonal basis, the branching ratio increases gradually as a function of γ_{fis}, even though the insensitivity property may be realized at large values of γ_{fis}. To check the dependence on the number of Q blocks, we repeat the calculations with $7Q$ blocks, parametrizing V as $V(q)/d = 4 - 4q^2/9$ ranging from $q = -3$ to $q = 3$ with $\Delta q = 1$. In this case, the branching ratio changes by less than a factor of two while the fission decay varies by an order of magnitude. All of these results indicate that the hypothesis used in the Bohr-Wheeler theory is easily realized in the present microscopic theory. See also Ref. [29] for a similar study with random matrices.

IV. SUMMARY

In this article, we have applied the CI methodology to a schematic model for neutron-induced fission. The model Hamiltonian contains the pairing interaction, the diabatic interaction, and a schematic off-diagonal neutron-proton interaction. The model appears to be sufficiently detailed to examine the sensitivity of the fission transmission probabili-

TABLE III. Estimated orbital level spacing in ^{236}U. The first two are from potential models and the last extracted from the Fermi gas formula and measured level densities.

d (MeV)	Source
0.45	Woods-Saxon well
0.51	FRLDM [31]
0.33	FGM [32]

ties to the different types of interaction, as well as the validity of transition state theory in a microscopic framework. We have shown that the transmission coefficients are mainly sensitive to the neutron-proton interaction, while the sensitivity to the pairing interaction is much milder. The diabatic transitions were also found to play a role. Depending on the interaction and the deformation-dependent configuration space, one achieves conditions in which branching ratios depend largely on barrier-top dynamics and are insensitive to properties closer to the scission point. The insensitive property is one of the main assumptions in the well-known Bohr-Wheeler formula for induced fission, but up to now it had no microscopic justification.

The results in this paper indicate that the neutron-proton interaction is an important part of a microscopic theory for induced fission. To include it in realistic calculations based on the density-functional theory will require a large model space, however. See Table III in Ref. [11] for some estimates of the dimensional requirements. Moreover, single-particle energies are in general not degenerate in contrast to the schematic model employed in this paper. This might require a different energy cutoff, further enlarging the model space. To carry out such large-scale calculations for induced fission, one will have to either validate an efficient truncation scheme or develop an efficient numerical method to invert matrices with large dimensions. We leave this for a future work.

APPENDIX A: ESTIMATION OF PHYSICAL PARAMETERS

1. Orbital energy spacing

The single-particle level spacing d in the uniform model sets the energy scale for the model and does not play any explicit role in the model. However, it is required to determine other energy parameters which are expressed in units of d. Several estimates of d for ^{236}U are given in Table III. The

TABLE IV. Characteristics of single-particle orbitals in a deformed Woods-Saxon potential corresponding to ^{236}U at deformation $(\beta_2, \beta_4) = (0.274, 0.168)$. Dashed lines indicate the Fermi level.

Protons			Neutrons		
$2K$	π	$\varepsilon_{K\pi}$ (MeV)	$2K$	π	$\varepsilon_{K\pi}$ (MeV)
3	-1	-3.39	5	-1	-4.15
5	-1	-3.80	1	-1	-4.25
5	1	-4.93	7	-1	-4.40
- - - - - -			- - - - - -		
1	1	-5.43	1	1	-5.07
9	-1	-5.53	5	1	-5.75
3	1	-5.74	5	-1	-5.82

TABLE V. Estimates of neutron-proton interaction strength.

Basis of estimate	v_0 (MeV fm^3)	Citation
G matrix	530	[21]
sd shell spectra	490	[35]
β decay	395, 320	[36]

first is based on orbital energies in a deformed Woods-Saxon potential with the parameters given in Ref. [30]; see Table IV for the calculated orbital energies. In more realistic theory, the momentum dependence of the potential tends to increase the spacing, but the coupling to many-particle degrees of freedom decreases the spacing of the quasiparticle poles. The combined effect seems to somewhat decrease the spacing.[2]

2. Level density

It is important to know the composition of the levels in the compound nucleus to construct microscopic models that involve those levels. For a concrete example, consider the levels at the neutron threshold energy $S_n = 6.5$ MeV in ^{236}U. The predominant configurations at this energy should be k subblocks at $k \approx S_n/d$ in the independent quasiparticle approximation. Another approach that is less sensitive to the residual interaction is to estimate the total number of states below S_n and compare it to the number obtained by summing the N_k degeneracies in the Q-block spectrum. In the ^{236}U example, the combined level spacing of $J^\pi = 3^-$ and 4^- is about 0.45 eV at S_n [34]. At that excitation energy the level density is the same for even and odd parities, and it varies with angular momentum as $2J + 1$. The inferred level spacing of $J^\pi = 0^+$ levels is thus about 7 eV. The accumulative number of levels can be approximated by $N = \rho T$ where T is the nuclear temperature, defined as $T = d \ln(\rho(E))/dE$. A typical estimate for our example is $T = 0.65$ MeV, giving $N \approx 1.0 \times 10^8$. To estimate the level density in the present model, we start with the set of quasiparticle configurations including both parities and all K values. The resulting k blocks have multiplicities that are well fit by the formula

$$N_k \approx \exp(-3.23 + 4.414 k^{1/2}). \tag{A1}$$

Projection on good parity decreases this by a factor of two. The projection on angular momentum $J = 0$ is more subtle. The $J = 0$ states are constructed by projection from $K = 0$ configurations; other configurations do not contribute. However, there may be two distinct configurations that project to

the same $J = 0$ state. This gives another factor of nearly two reduction in the multiplicity. The remaining task is to estimate the fraction of $K = 0$ configurations in the unprojected quasiparticle space. The distribution of K values is approximately Gaussian with a variance given by

$$\langle K^2 \rangle = \langle n_{\mathrm{qp}} \rangle \langle K^2 \rangle_{\mathrm{sp}}, \tag{A2}$$

where $\langle n_{\mathrm{qp}} \rangle \approx 8$ is the average number of quasiparticles in the k block and $\langle K^2 \rangle_{\mathrm{sp}} \approx 6$ is an average over the orbital Ks near the Fermi level. Including these projection factors, the integrated number of levels up to S_n is achieved by including all k subblocks up to $k = 17$ in the entry Q block.

3. Neutron-proton interaction

To set the scale for our neutron-proton interaction parameter v_{np} we compare it with phenomenological contact interactions that have been used to model nuclear spectra. The matrix element of the neutron-proton interaction is

$$\langle n_1 p_1 | v | n_2 p_2 \rangle = -v_0 I, \tag{A3}$$

where

$$I = \int d^3 r \phi_{n_1}^*(\boldsymbol{r}) \phi_{p_1}^*(\boldsymbol{r}) \phi_{n_2}(\boldsymbol{r}) \phi_{p_2}(\boldsymbol{r}). \tag{A4}$$

The parameter v_0 is the strength of the interaction, typically expressed in units of MeV fm^3. Some values of v_0 from the literature are tabulated in Table V. We shall adopt the value $v_0 = 500$ MeV fm^3 to estimate the value of v_{np}.

If the wave functions of the eigenstates approach the compound nucleus limit, the only characteristic we need to know is its mean-square average among the active orbitals. We have used the Woods-Saxon model to calculate the integral Eq. (A4) for all the fully off-diagonal matrices of the orbitals within 2 MeV of the Fermi energy. Figure 6 shows a histogram of their distribution.[3] The variance of the distribution is $\langle I^2 \rangle^{1/2} = 5.22 \times 10^{-5}$ fm^{-3}. Combining this with our estimate of v_0 we find $(\overline{\langle n_1 p_1 | v | n_2 p_2 \rangle^2})^{1/2} = 0.025$ MeV. This implies $v_{\mathrm{np}} \sim 0.05d$ with our estimated single-particle level density.

APPENDIX B: REACTION THEORY IN A NONORTHOGONAL BASIS

The space of configurations used in this work is not orthogonal. This causes some conceptual issues but does not cause a significant computational burden in CI-based reaction theory.

---

[2]We note that an energy density functional fit to fission data [33] obtained an effective mass in the single-particle Hamiltonian very close to 1.

---

[3]If the orbitals are restricted only to those in Table IV, the histogram is more structured
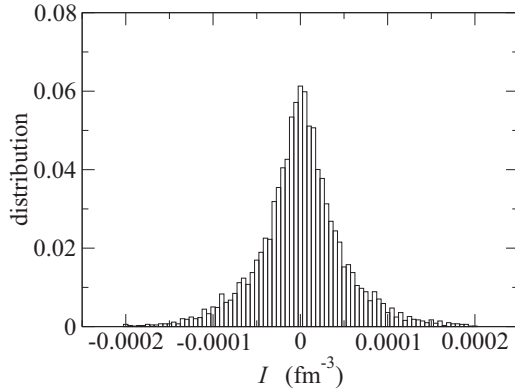
FIG. 6. Integrals I in Eq. (A4) of orbitals near the Fermi energy.

The theory is based on calculating the resolvent of H; in an orthogonal basis it is given by

$$G = (H - E\mathbb{1})^{-1}, \tag{B1}$$

where $\mathbb{1}$ is the unit matrix, H is the Hamiltonian, and E is the energy of the reaction. Non-orthogonal bases also arise in the theory of spontaneous decays [37], and in electron transport theory when wave functions are built from atomic orbitals. See, for example, Refs. [38–42] for the formulation of the resolvent as commonly used in chemistry and condensed-matter physics.

In a nonorthogonal basis the time-dependent Schrödinger equation reads

$$H\Psi = i\hbar N \frac{d}{dt}\Psi, \tag{B2}$$

where N is the overlap matrix between basis states $N_{ij} = \langle i | j \rangle$. The corresponding resolvent is

$$G = (H - EN)^{-1}. \tag{B3}$$

There is hardly any difference from Eq. (B1) from a computational point of view. However, the couplings to reaction channels should be treated with care.

To understand the couplings, we define a certain orthogonal basis which we call the physical basis. We call the vector representing a wave function in that basis $\boldsymbol{v}_{\text{phys}}$ and in the nonorthogonal basis, $\boldsymbol{v}_{\text{gcm}}$. In the GCM the dot products of basis elements satisfy

$$\boldsymbol{v}_{\text{gcm}}(i)^* \cdot \boldsymbol{v}_{\text{gcm}}(j) = N_{ij}, \tag{B4}$$

while those in the physical basis satisfy

$$\boldsymbol{v}_{\text{phys}}(i)^* \cdot \boldsymbol{v}_{\text{phys}}(j) = \delta_{ij}. \tag{B5}$$

A physical basis consistent with Eq. (B4) can then be defined by setting

$$\boldsymbol{v}_{\text{phys}}(i) = \sum_j N_{ij}^{1/2} \boldsymbol{v}_{\text{gcm}}(j). \tag{B6}$$

This definition is not unique since the dot products are invariant under a unitary transformation of the physical basis. Indeed, an orthogonal basis is usually constructed in the GCM by diagonalizing N and using its eigenvectors as the basis.

However, those basis states are not well localized with respect to the GCM coordinate.

The relationship between the Hamiltonians in the physical and GCM bases can be expressed

$$\tilde{H} = N^{-1/2} H N^{-1/2} \tag{B7}$$

or

$$H = N^{1/2} \tilde{H} N^{1/2}. \tag{B8}$$

The physical resolvent is related to the GCM resolvent by

$$\tilde{G} = (N^{-1/2} H N^{-1/2} - E\mathbb{1})^{-1}$$
$$= N^{1/2}(H - EN)^{-1} N^{1/2}. \tag{B9}$$

One see that the matrix inversion is the same as in Eq. (B1) except for the replacement $\mathbb{1} \to N$. However, the matrix $N^{1/2}$ appears as pre- and postfactors.

In our applications of CI-based reaction theory we assume that each channel is coupled to a single state (the "doorway" state) in the internal space. Taking that state to be the basis state d in the physical representation, the decay coupling matrix Γ has elements[4]

$$\Gamma(i, j) = N_{id}^{1/2} N_{jd}^{1/2} \tilde{\Gamma}, \tag{B10}$$

where $\tilde{\Gamma}$ is the decay width of the physical state d into the channel. Note that with this construction the transmission coefficient in the physical basis

$$T_{a,b} = \text{Tr}[\tilde{\Gamma}_a \tilde{G}(E) \tilde{\Gamma}_b \tilde{G}^\dagger(E)] \tag{B11}$$

is transformed to

$$T_{a,b} = \text{Tr}[\Gamma_a G(E) \Gamma_b G^\dagger(E)] \tag{B12}$$

in the GCM basis.

There is another reason for explicit construction of the physical basis. The distinction between the GCM and physical basis must be taken into account in Sec. III B where we assessed the relevant importance of different interaction types and we want to start with a Hamiltonian $\tilde{H}^0$ for which the transmission probability vanishes. One cannot simply set the off-diagonal elements of H to zero if the overlap matrix N connects the entrance and exit channels, even if the connection is indirect. It is the physical Hamiltonian $\tilde{H}$ that must be diagonal. In two dimensions the construction is obvious. Given the diagonal elements of $H(i, i) = E_i$, the Hamiltonian that is diagonal in the physical basis is

$$H^0 = \begin{pmatrix} E_1 & (E_1 + E_2)N_{12}/2 \\ (E_1 + E_2)N_{12}/2 & E_2 \end{pmatrix}. \tag{B13}$$

Eq. (B13) can be viewed as a justification for the first term in Eq. (9). The construction can be carried out in higher dimensions using only linear algebra operations, but we have no simple formula for the off-diagonal elements of H^0. For

---

[4] A somewhat similar formula was used in Ref. [[10], Eq. (16)].

the base Hamiltonian treated in Sec. III B, N is given by

$$N = \begin{pmatrix} 1.0 & e^{-1} & e^{-4} \\ e^{-1} & 1.0 & e^{-1} \\ e^{-4} & e^{-1} & 1.0 \end{pmatrix}. \quad \text{(B14)}$$

Keeping only $V(q)$ in H, H^0 is numerically found to be

$$H^0 = \begin{pmatrix} 0.0000 & 0.7571 & 0.1537 \\ 0.7571 & 4.000 & 0.8547 \\ 0.1537 & 0.8547 & 0.5000 \end{pmatrix}. \quad \text{(B15)}$$

[1] O. Hahn and F. Strassmann, Naturwissenschaften **27**, 11 (1939).
[2] R. Vandenbosch and J. R. Huizenga, *Nuclear Fission* (Academic Press, New York, 1973).
[3] N. Bohr and J. A. Wheeler, Phys. Rev. **56**, 426 (1939).
[4] W. Hauser and H. Feshbach, Phys. Rev. **87**, 366 (1952).
[5] J. Randrup and P. Möller, Phys. Rev. Lett. **106**, 132503 (2011).
[6] Y. Aritomo, S. Chiba, and F. Ivanyuk, Phys. Rev. C **90**, 054609 (2014).
[7] C. Ishizuka, M. D. Usang, F. A. Ivanyuk, J. A. Maruhn, K. Nishio, and S. Chiba, Phys. Rev. C **96**, 064616 (2017).
[8] K. H. Schmidt and B. Jurado, Rep. Prog. Phys. **81**, 106301 (2018).
[9] M. Bender *et al.*, J. Phys. G **47**, 113002 (2020).
[10] G. F. Bertsch and K. Hagino, Phys. Rev. C **105**, 034618 (2022).
[11] G. F. Bertsch and K. Hagino, Phys. Rev. C **107**, 044615 (2023).
[12] P. Ring and P. Schuck, *The Nuclear Many-Body Problem* (Springer-Verlag, Berlin, 2000).
[13] F. Dönau, J. Zhang, and L. Riedinger, Nucl. Phys. A **496**, 333 (1989).
[14] G. F. Bertsch and K. Hagino, arXiv:2102.07084.
[15] S. Datta, *Electronic Transport in Mesoscopic Systems* (Cambridge University Press, Cambridge, 1995).
[16] Y. Alhassid, G. F. Bertsch, and P. Fanto, Ann. Phys. (NY) **419**, 168233 (2020).
[17] Y. Alhassid, G. F. Bertsch, and P. Fanto, Ann. Phys. (NY) **424**, 168381 (2021).
[18] M. Barbui, A. Volya, E. Aboud, S. Ahn, J. Bishop, V. Z. Goldberg, J. Hooker, C. H. Hunt, H. Jayatissa, Tz. Kokalova, E. Koshchiy, S. Pirrie, E. Pollacco, B. T. Roeder, A. Saastamoinen, S. Upadhyayula, C. Wheldon, G. V. Rogachev, Phys. Rev. C **106**, 054310 (2022).
[19] D. M. Brink and R. A. Broglia, *Nuclear Superfluidity: Pairing in Finite Systems* (Cambridge University Press, Cambridge, 2005).
[20] G. F. Bertsch, Phys. Rev. C **101**, 034617 (2020).
[21] B. W. Bush, G. F. Bertsch, and B. A. Brown, Phys. Rev. C **45**, 1709 (1992).
[22] K. Hagino and G. F. Bertsch, Phys. Rev. C **105**, 034323 (2022).
[23] G. F. Bertsch and L. M. Robledo, Phys. Rev. C **100**, 044606 (2019).
[24] G. F. Bertsch and T. Kawano, Phys. Rev. Lett. **119**, 222504 (2017).
[25] S. A. Giuliani, L. M. Robledo, and R. Rodriguez-Guzman, Phys. Rev. C **90**, 054311 (2014).
[26] J. Sadhukhan, J. Dobaczewski, W. Nazarewicz, J. A. Sheikh, and A. Baran, Phys. Rev. C **90**, 061304(R) (2014).
[27] R. Rodríguez-Guzmán and L. M. Robledo, Phys. Rev. C **98**, 034308 (2018).
[28] F. Barranco, G. Bertsch, R. Broglia, and E. Vigezzi, Nucl. Phys. A **512**, 253 (1990).
[29] G. F. Bertsch and K. Hagino, J. Phys. Soc. Jpn. **90**, 114005 (2021).
[30] A. Bohr and B. R. Mottelson, *Nuclear Structure* (W. A. Benjamin, Reading, 1969), Vol. I.
[31] P. Möller *et al.*, At. Data Nucl. Data Tables **59**, 185 (1995); private communication (P. Möller).
[32] A. J. Koning, S. Hilaire, and S. Goriely, Nucl. Phys. A **810**, 13 (2008).
[33] M. Kortelainen, J. McDonnell, W. Nazarewicz, P. G. Reinhard, J. Sarich, N. Schunck, M. V. Stoitsov, and S. M. Wild, Phys. Rev. C **85**, 024304 (2012).
[34] R. Capote *et al.*, Nucl. Data Sheets **110**, 3107 (2009).
[35] B. A. Brown *et al.*, Ann. Phys. (NY) **182**, 191 (1988).
[36] K. Yoshida, Prog. Theor. Exp. Phys. **2013**, 113D02 (2013).
[37] K. Hagino and G. F. Bertsch, Phys. Rev. C **102**, 024316 (2020).
[38] M. G. Reuter, T. Seideman, and M. A. Ratner, Phys. Rev. B **83**, 085412 (2011).
[39] O. Hod, J. E. Peralta, and G. E. Scuseria, Phys. Rev. B **76**, 233401 (2007).
[40] O. Hod, J. Peralta, and G. E. Scuseria, J. Chem. Phys. **125**, 114704 (2006).
[41] A. Pecchia and A. Di Carlo, Rep. Prog. Phys. **67**, 1497 (2004).
[42] M. Buongiorno Nardelli, Phys. Rev. B **60**, 7828 (1999).